ORIGINAL PAPER

Electrolysis energy efficiency of highly concentrated FeCl$_2$ solutions for power-to-solid energy storage technology

Uroš Luin[1] · Matjaž Valant[1]

Abstract

An electrochemical cycle for the grid energy storage in the redox potential of Fe involves the electrolysis of a highly concentrated aqueous FeCl$_2$ solution yielding solid iron deposits. For the high overall energy efficiency of the cycle, it is crucial to maximize the energy efficiency of the electrolysis process. Here we present a study of the influence of electrolysis parameters on the energy efficiency of such electrolysis, performed in an industrial-type electrolyzer. We studied the conductivity of the FeCl$_2$ solution as a function of concentration and temperature and correlated it with the electrolysis energy efficiency. The deviation from the correlation indicated an important contribution from the conductivity of the ion-exchange membrane. Another important studied parameter was the applied current density. We quantitatively showed how the contribution of the resistance polarization increases with the current density, causing a decrease in overall energy efficiency. The highest energy efficiency of $89 \pm 3\%$ was achieved using 2.5 mol L^{-1} FeCl$_2$ solution at 70 °C and a current density of 0.1 kA m^{-2}. In terms of the energy input per Fe mass, this means 1.88 Wh g^{-1}. The limiting energy input per mass of the Fe deposit was found to be 1.76 Wh g^{-1}.

Keywords Electrolysis · Ferrous chloride · Iron deposition · Energy efficiency

Introduction

The shift to renewable sources of energy is beginning to expose a fundamental weakness in the world's electricity grids. Solar, wind, wave, and other forms of renewable energy are all, to some extent, subject to the vagaries of factors like the weather [1]. This means that we cannot match the amounts of energy available with demand, because we do not have an effective way to store and then release this energy when we need it. Globally speaking, the problem is not a shortage of energy; it is primarily that of energy storage [2, 3]. Existing energy storage systems all suffer fundamental weaknesses: they lack long-term stability, like batteries; they are geographically limited, like pumped storage hydropower; they suffer from low efficiencies, like compressed-air energy storage; or they are economically

non-viable, like converting electricity into fuel. We need a storage method that overcomes all the above limitations.

A novel power-to-solid (P-to-S) energy storage technology that tackles this problem is based on electrolysis of FeCl$_2$ aqueous solution [4]. In short, the technology enables long-term grid energy storage without self-discharge. The energy is stored in the oxidative-reductive potential change of iron (Fe^{2+}/Fe). This is obtained by the electrolytic reduction of Fe^{2+} from a highly concentrated FeCl$_2$ (aq) electrolyte yielding metallic iron that deposits on the cathode. Simultaneously, on the anode chlorine gas evolves, which is further subjected to conversion to HCl acid using a reversed Deacon process [5]. Energy is released via the on-demand generation of hydrogen obtained from a spontaneous reaction between the iron and HCl acid. The entire process is modular and upscale-able, and runs in a materially closed cycle with no emission, waste, or material consumption. For the optimum energy efficiency of the technology, optimization of the electrolytic process is crucial.

Nowadays, the electrolysis cells with a selectively permeable membrane are the preferred type as they substitute two environmentally harmful options used in the past; that are mercury cells and asbestos diaphragm cells [6]. In

✉ Matjaž Valant
matjaz.valant@ung.si

Uroš Luin
uros.luin@ung.si

1 Materials Research Laboratory, University of Nova Gorica, Vipavska 13, 5000 Nova Gorica, Slovenia

addition, they are 30% more energy efficient as reported for the chlor-alkali process [7, 8]. There are also possible drawbacks such as higher maintenance or operating costs for the replacement of degraded membranes and the need for high purity electrolytes required for preventing fouling [9]. Moreover, the same authors proposed future development towards self-cleaning and non-fouling membranes or to allow removal of the precipitates from the membrane during process downtime. The last idea is fully applicable to the P-to-S technology, since there is, by the principle, downtime between the energy storage and release available.

For the high current (or Faraday) efficiency of the aqueous solution electrolysis, it is essential to avoid unwanted secondary reactions such as water splitting. In contrast, the electrolysis systems using non-aqueous electrolytes have been studied, mostly to limit the secondary reactions and unwanted effects on deposited film morphology occurring due to hydrogen embrittlement [10–13]. The drawbacks of the non-aqueous electrolytic organic media are low conductivity due to low solubility of ionic metal species, consequently lower electrolysis energy efficiency, electrolyte drag-out due to high viscosity, flammability, and relatively high cost [14, 15]. The electrochemical behavior of iron has also been studied in chloro-aluminate [16, 17], chloro-zincate ionic liquids [18], and molten salts [19, 20].

Aqueous solutions of salts have much lower conductivity than aqueous solutions of strong acids. For example, $ZnCl_2$ solution (25 °C) reaches a conductivity peak of 107 mS cm^{-1} at 3.7 mol L^{-1} [21], whereas the conductivity of 10% wt HCl (aq) is much higher, ~710 mS cm^{-1} at 25 °C. This is due to the nature of proton-hopping transport in the aqueous media known as the Grotthuss mechanism [22, 23]. Furthermore, the presence of the HCl acid in the aqueous $FeCl_2$ improves stability [24, 25] and increases the conductivity. But, at the same time, a rather minor acid addition drops the pH of the electrolyte low enough to trigger an unwanted hydrogen evolution reaction (HER) during the electrolysis.

Besides HER, another possible contribution to the decrease in the electrolysis energy efficiency comes from the oxidation of the ionic Fe (II) to Fe (III). Based on cyclic voltammetry experiments of Fe (III) salt, [26] a well-defined cathodic wave was reported in the potential range between −0.2 and −1.2 V vs. Ag|AgCl, confirming that before the Fe deposition, the reduction of Fe (III) into Fe (II) occurs. Although dealing with a pure ferrous chloride catholyte, the oxidation may happen through oxygen intrusion into the catholyte and/or a membrane failure leading to diffusion of oxidative species from the anolyte into the catholyte compartment. All of these could be sufficiently avoided by using relatively simple measures. First, it is important to keep catholyte pH > 2, since the HER rate gradually decreases with an increase in pH [27–29]. Next, the oxygen intrusion

is sufficiently prevented by applying slight overpressure of inert gas to the catholyte hydraulic circuit.

The selection of anode material is important for continuous operation with high efficiency. A stable anode exhibits no significant degradation or weight loss over reasonable working time. The research and development of the chlorine evolution anodes started in the 1950s [30] and by today resulted in the development of dimensionally stable anodes (DSA De Nora trademark, hereafter DSA®) based on titanium with a rare metal oxide coating [31, 32]. DSA® is characterized by a good performance at high current densities, a low overpotential for chlorine evolution, and good selectivity for the chlorine over oxygen evolution reaction [32–34]. Depending on the design and type, DSA® operates at current densities up to 4 kA m^{-2} [35]. Commercially available DSA® are mostly mixed metal oxide titanium anodes with an $IrO_2 - RuO_2$-TiO_2-type coating containing one or several dopant materials [33, 34, 36]. They operate at the potential of about 1.36 V vs. NHE [37]. Due to the content of rare and precious materials, and consequently expensive DSA® anodes, it is mandatory to operate the electrolysis under safe conditions to avoid degradation. On the other hand, for industrial applications, it is important to operate at as high as possible current densities. So, optimization of the operation performance must be considered.

The majority of the research work on the electrolysis of $FeCl_2$ solutions has so far focused on either optimization of the deposit properties or rapid Fe extraction, rather than on the efficiency [38–41]. For that reason, many studies have been performed at either very high $FeCl_2$ concentrations or very high current density. In contrast, our primary aim is to optimize the energy efficiency while the deposit properties are of secondary concern because the reaction, of the iron and HCl acid, in all cases runs quite vigorously to 100% completeness yielding the theoretical stoichiometric amount of the H_2.

Concentrations as high as 725 g L^{-1} $FeCl_2 \cdot [4H_2O]$ (~3.65 mol L^{-1} $FeCl_2$) have been used for the studies of low-stress deposits [42]. However, at such high concentrations, the ionic interactions are already high and, so, far away from the peak conductivity. Reported are iron deposition studies performed at very high current densities, > 4 kA m^{-2}, and up to 60 kA m^{-2} [41, 43]. Nevertheless, under such conditions energy efficiency significantly drops due to pronounced losses. In addition, at high current density, the current efficiency is reduced due to secondary reactions, in particular the HER. Therefore, to obtain a significantly higher current efficiency (> 95%) and thus keep the energy efficiency high, we designed our electrolysis system to operate in the current density range up to 2 kA m^{-2}.

The process of iron electrodeposition from aqueous $FeCl_2$ solution has also been studied for iron and chlorine recovery from industrial wastewaters, in which the $FeCl_2$

concentration is relatively low [44, 45]. Despite the similarity, these processes are not designed and optimized for energy storage purposes. In other words, the electrolyzer construction and the electrolysis parameters were not fully optimized for energy efficiency, since the technological purpose was different, predominantly targeting the deposit properties. However, they still provide valuable information and allow some empirical comparison. In particular, the authors claim that current efficiency was > 90% and energy consumption was in the range of 2.1–6.2 Wh g^{-1} [45]. The electrodeposited iron from FeCl$_2$ aqueous solution is highly pure (> 99%) [39] and, importantly, also fairly corrosion-resistant when the rinsing of the remaining electrolyte from the deposit is sufficient [38, 43].

For the P-to-S technology, it is important to maximize the electrolysis energy efficiency of the highly concentrated FeCl$_2$ solution concerning the technology-relevant parameters such as the applied potential, current density, working temperature, and catholyte concentration. Furthermore, the conditions that are causing secondary reactions or the degradation of the system parts must be avoided. As explained above, the previous studies of the electrolytic processes in such catholyte systems have focused on either low salt concentrations or optimization of current efficiency due to the requirements of the intended applications. Energy efficiency has not been the key parameter as it is in the case of energy storage technology. For this reason, we have studied the influence of the operating parameters on the electrolysis energy efficiency of the highly concentrated FeCl$_2$ solutions to maximize it.

Methodology

Electrolyzer

We used a modified industrial-type small-size chlor-alkali electrolyzer (ChemTech Engineering S.r.l., Italy) (Fig. 1). A single electrolytic cell was used for the experiments presented in this paper. The electrolytic cell consists of two half-cell compartments separated by anion exchange membrane AMI7001s (Membrane International Inc.). Each half-cell compartment is around 1 dm^3 in volume. The cathode is a titanium mesh welded to a titanium frame. Similarly, the anode is titanium mesh coated with mixed metal oxide film used for the evolution of chlorine gas in the chlor-alkali industry (De Nora DSA®). The housing of the half-cells is made of PTFE (polytetrafluoroethylene). The seals between the components are made of a 3-mm-thick EPDM (ethylene propylene diene monomer) rubber gasket. The cell components are compressed in a dedicated six-point stainless steel (AISI304) clamping press. The outer side dimension of the square electrolysis cell is 300 mm, while the inner is 250 mm.
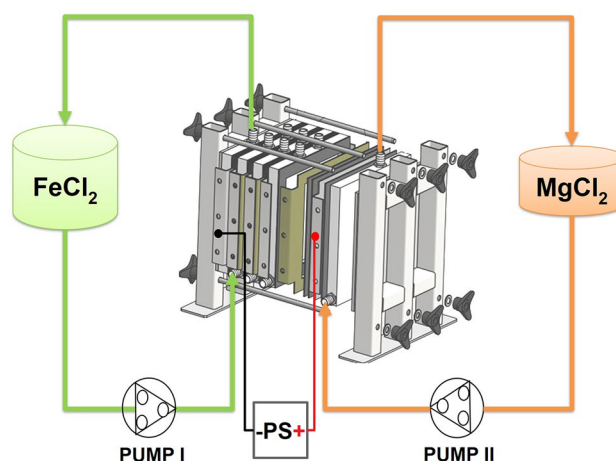
Fig. 1 The diagram of the experimental electrolysis system; the electrolyzer unit with several electrolytic cells mounted in the press-like frame to assure hydraulic tightness; the catholyte cycle (green arrows); the anolyte cycle (orange arrows); + PS- represents the DC power supply with electrical connections

A non-conductive masking tape is placed on the inner edge of the EPDM seal toward the direction of the membrane. The cell-active cross-sectional area is 0.0552 m^2. The distance between the electrodes is roughly 3 mm.

Due to the evolution of gaseous products, a bottom-up flow through the half-cell compartments was applied using two peristaltic pumps (Boxerpumps 25 K-3RWT1.6). In the anolyte hydraulic circuit, a mixture of liquid and gas enters the tank. The electrolyte tanks also function as a degassing unit. The gasses leave the system, while the liquid phase re-enters through the lower inlet of the electrolytic cell. During the electrolysis, the catholyte concentration decreases because of the iron deposition on the cathode. The stock catholyte volume was oversized to ensure that the concentration remains within the target optimal conductivity range for the whole duration of the experiments.

Before the start of the electrolysis, the system was preheated, which includes preheating of the tanks with electrolytes, massive steel frame, and PTFE cell parts. The electrolyte circulation assured even temperature through the system. The thermocouple was immersed in the catholyte tank at the inlet flow coming from the electrolytic cell.

Electrolytes

Deionized water (Grade 2) was used for all the prepared electrolytes. The measurements of the pH, conductivity, and temperature were performed using Phoenix EC45-Multi probes linked to a PC data-logging software. The measuring cell, Sentek VPT80C10, was calibrated using Hamilton ZDL 300 mL standard solution with a conductivity of 100 mS cm^{-1} at 25 °C. The used pH probe (XS S7) was 3

points calibrated. For all the experiments, an aqueous solution of 20% wt $MgCl_2$, prepared from $MgCl_2 \cdot 6H_2O$ (Fisher Chem.), with a pH 1 ± 0.2 was used as the anolyte. $MgCl_2$ was selected to keep the concentration of the cations in the anolyte compartment low and yet assure the conductivity higher than that of the catholyte. The anolyte pH was adjusted using 25% wt HCl acid (Acros Organics, analysis grade).

The $FeCl_2$ (aq) solutions used as catholyte were prepared from $FeCl_2 \cdot 4H_2O$ (Acros Organics). To compensate for depleted concentration after each experiment, an appropriate amount of $FeCl_2 \cdot 4H_2O$ was added. In the presented experiments, we used 1, 2.5, and 4 mol L^{-1} $FeCl_2$ concentrations for the catholyte. The catholyte concentration was verified through conductivity measurements. The solutions were stored in air-tight transparent borosilicate glass bottles under a nitrogen gas atmosphere at room temperature. Such an approach prevents oxidation of Fe (II) if the glassware is tightly closed and no oxygen is present.

Anion exchange membrane (AEM)

The specified hydration procedure proposed by AEM manufacturers was followed before use. This requires immersing the AEM in 5% wt NaCl aqueous solution for 72 h and transferring it to a freshly prepared storage solution (5% wt NaCl (aq)). After each experiment, the membrane was immediately immersed into a cleaning solution (~3% wt HCl) for 12–36 h, and then rinsed with demineralized water and immersed in the storage solution until the next experiment. Just before mounting in the electrolyzer, the membrane was taken out of the storage solution, rinsed with deionized water, and shortly flushed with a moderate nitrogen flow to avoid NaCl entering the system.

Performance of the experiments

For each experiment, the following steps were applied:

– The precise weighting of the clean and dry cathode without EPDM rubber gasket as well without any trace of iron deposit from the previous experiment.
– A purge of the catholyte hydraulic circuit with nitrogen gas (5.0 purity) for 15–30 min at flow > 100 L h^{-1}. During the experiment, the nitrogen gas flow was reduced to around 10 L h^{-1}.
– System preheating includes electrolytes, massive press metal frame, and PTFE parts of the electrolytic cell. The temperature was monitored before and during the electrolysis by a thermocouple installed directly in the

catholyte tank on the inlet spot of the return flow from the electrolyzer.
– Once the target temperature of electrolytes was achieved, the anion exchange membrane was installed. This was done just before starting the circulation of the electrolytes over peristaltic pumps.
– Initialization (polarization) procedure at zero net current and E^0 potential via constant current power supply mode, for the period of temperature stabilization (typically 10 to 20 min).
– The duration of the electrolysis experiment was adjusted to a total charge transfer of 30 Ah.

Energy input (E_{input}) was derived from the integration of current and voltage over electrolysis operation time as shown in Eq. (1).

$$E_{input} = \int U \cdot I \cdot dt \tag{1}$$

where U, I, and t are voltage, current, and time, respectively.

The voltage and current were precisely measured using double handheld Keysight U1282A multi-meters linked to PC via Keysight handheld meter logger software equipment. The voltage was measured directly across the electrodes to avoid the voltage drop due to the Ohmic resistance of the supplying cables (length: 5 m, cross-section area: 50 mm^2). The current was derived from the voltage drop over a brass DC Shunt resistor (FL-19B 75 mV 100A) placed 2 cm from the cathode on the (negative) supplying cable. The datalogger recording interval was set to 1 s.

The energy efficiency (η_e), as shown in Eq. (2), is defined as the ratio between Gibbs free energy changes for the overall electrolytic process multiplied by the amount of produced iron (mol_{Fe}) per energy consumed during electrolysis (E_{Input}). The Gibbs free energy change ($-\Delta G^0$), calculated according to Eq. (3), is 348.4 kJ mol^{-1}.

$$\eta_e = \frac{|\Delta G^0| \cdot mol_{Fe}}{E_{Input}} \tag{2}$$

$$-\Delta G^0 = nFE^0 \tag{3}$$

where F, n, E^0, and mol_{Fe} are Faraday constant, the number of electrons ($n = 2$), and molar amount of deposited iron, respectively. The standard cell potential, E^0_{cell}, is 1.805 V at 25 °C.

When the electrolysis finished, the cathode was removed from the cell, the deposit was immediately rinsed (to remove electrolyte traces) with deionized water, isopropanol, nitrogen gas purged, and dried. The exact amount of the electrodeposited iron was obtained by weighting the cathode before and after the experiment.

Results and discussion

### Conductivity of the catholyte (Fig. 2)

The first part of the experimental work has focused on efficiency optimization through the maximization of the electrolytic cell conductivity. The first step towards this goal is a detailed study of the properties of the electrolyte that includes the studies of electrolyte conductivity as a function of electrolyte concentration and temperature. Initially, we measured the $FeCl_2$ solutions in the concentration range from 0.5 to 4.5 mol L^{-1} at 25 °C and obtained the curve with a shape typical for the inorganic salt solutions. The electrolytic conductivity increases with the concentration up to about 2 mol L^{-1} and starts falling with a further increase in the concentration. This is explained by the fact that the assumption of independent migration of ions is not valid for the highly concentrated solutions, for which the high ion-ion interactions prevail and reduce the conductivity (κ). This is a characteristic behavior of the majority of highly concentrated strong electrolytes and not constrained to a specific ion species population. The maximum conductivity was measured to be 143 mS cm^{-1} at the concentration of 2.25 mol L^{-1}. The solutions with the lowest and highest $FeCl_2$ concentration showed much smaller

conductivity of about 113 mS cm^{-1} and 98 mS cm^{-1}, respectively. In addition, measurements of the temperature dependence of the conductivity for the selected concentrations showed a very steep increase in conductivity. Mainly, such aqueous electrolytes exhibit the thermal coefficient of electrolytic conductivity ($\gamma = {}^{\Delta\kappa}/_{\Delta T}$) around 2.0 K^{-1} [46]. However, for the $FeCl_2$ solution, we have measured higher as expected. The highest was measured to be 2.84 K^{-1} for 2 mol L^{-1} solution, which undoubtedly shows a change in the population of ionic species and/or their solvation. The investigation of this phenomenon is presented and explained in a separated study [47].

Catholyte concentration

Based on the above results, we have performed electrolysis experiments to establish how much the catholyte concentration influences the efficiency of the electrolysis. Figure 3 shows the dependence of the current efficiency (upper figures) on the electrolyte concentration as a function of the potential and the dependence of the current density on the potential (bottom figures). In the majority of cases, the current efficiencies were close to 100%, but a significant drop occurred at the highest current density for 4 mol L^{-1} due to the observed secondary HER.

Fig. 2 The 3D plot shows the relation between conductivity, concentration, and temperature for the $FeCl_2$ aqueous solution
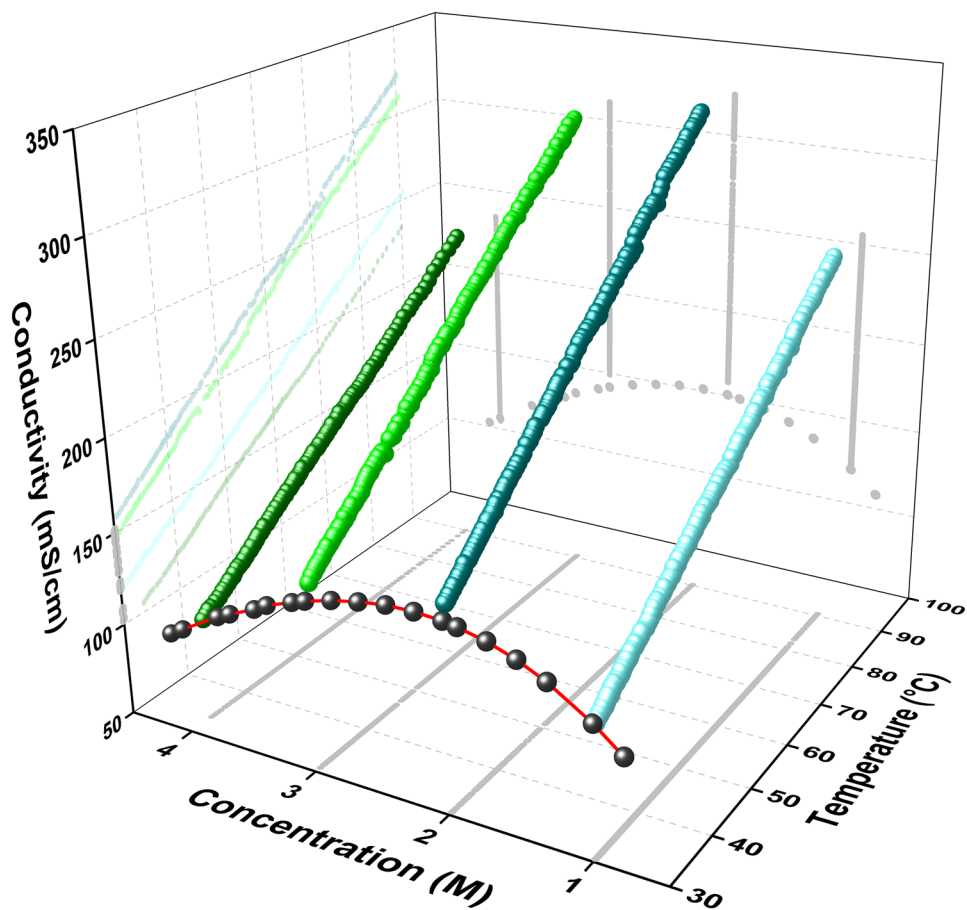
Fig. 3 The current efficiencies and current densities as a function of catholyte concentration and potential at a system temperature of 72 ± 2 °C
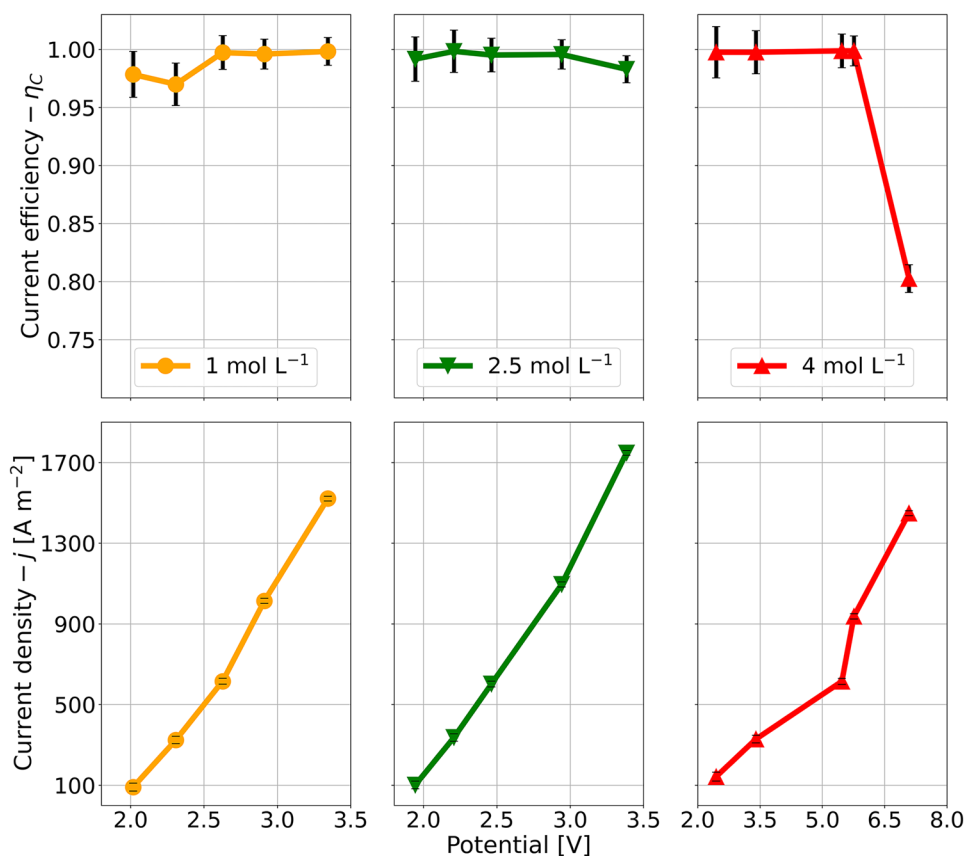
Interestingly, as shown in Fig. 4 the energy efficiency of 1 mol L^{-1} $FeCl_2$ is similar to that of the 2.5 mol L^{-1}, despite much lower conductivity (see Fig. 1). The electrolyte conductivity is not the only parameter that controls the energy efficiency of the electrolysis of the highly concentrated $FeCl_2$ solutions. This is even more evident by comparing 1 mol L^{-1} and 4 mol L^{-1} catholyte, in which conductivities are comparable. The 4 mol L^{-1} catholyte requires a significantly higher potential for the same
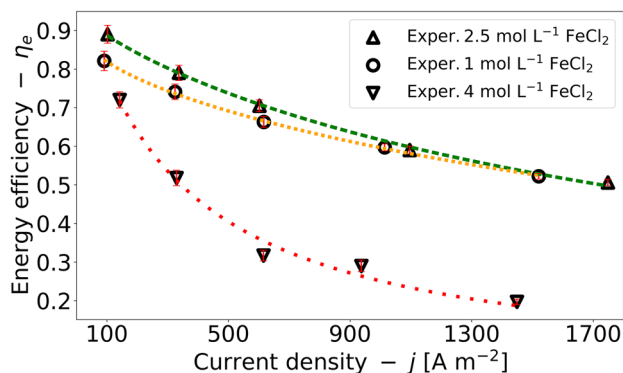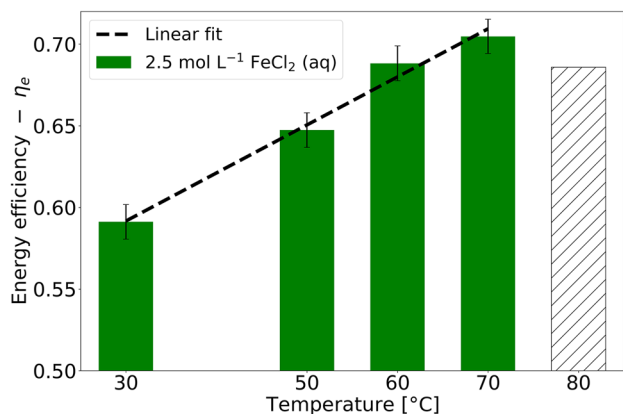

Fig. 4 Current density vs. energy efficiency relation for three different catholyte concentrations at 70 °C. The dashed lines represent the best fits obtained by using Eq. (4)

current density. Consequently, the electrolysis efficiency was much lower. The conductivity of metal electrodes is incomparably higher than the conductivity of electrolyte or membrane, so the reason for this behavior can only be in the performance of the ion-exchange membrane, in which resistivity increases with the $FeCl_2$ concentration due to an increase in ionic steric impediment [48–50]. This compensates for the increase in the catholyte conductivity from 1 to 2.5 mol L^{-1}. For the higher electrolyte concentrations, the simultaneous drop in the electrolyte and membrane conductivities results in a sharp decrease in energy efficiency. The Ohmic resistance of the electrolyzer at 70 °C and current density of 600 A m^{-2} was calculated based on experimental results to be 101 ± 5 mΩ for the catholyte concentration of 2.5 mol L^{-1} and 108 ± 5 mΩ for 1 mol L^{-1}. At the same conditions, the cell resistance for 4 mol L^{-1} was calculated to be 165 ± 5 mΩ.

System temperature

In the next set of experiments, we took the catholyte with the concentration of 2.5 mol L^{-1} that gives one of the best energy efficiency values at 25 °C and performed the electrolysis at elevated temperatures (30, 50, 70, 80 °C) and a current density of 600 ± 10 A m^{-2}. The temperature directly as well as indirectly impacts the electrolyte conductivity (see

Fig. 5 The electrolysis energy efficiency as a function of system temperature at 2.5 mol L^{-1} initial catholyte concentration and a current density of 600 ± 10 A m^{-2}

Fig. 2) due to changes in viscosity, ion mobility, ion-pair dissociation, electrolytes solubility, electrode wettability, amounts of dissolved gasses, standard reduction potential, etc. The results (Fig. 5) showed an increase in the energy efficiency by about 12% with an increase in temperature for 40 °C (30–70 °C). In our electrolyzer system, the oxidation of the catholyte Fe^{2+} ions to Fe^{3+} occurred at ≥ 80 °C. The oxidation was noticed as a change in the catholyte color from green to yellowish and precipitation of fine yellow-orange particles that were masking the membrane as well as the cathode surface. The oxidation has slightly (~3%) lowered the current efficiency because three electrons instead of two electrons were consumed to fully reduce iron cations electrochemically. Therefore, the drop in the energy efficiency was a combination of the increased potential due to masking particles and a drop in the current efficiency. Thus, to maximize the energy efficiency, the highest possible temperature should be applied, but care must be taken to prevent oxidation of the catholyte solution.

Current density

The highest energy efficiency of $89 \pm 3\%$ was obtained for the 2.5 mol L^{-1} catholyte at 0.1 kA m^{-2}. The efficiency monotonically dropped to $50.6 \pm 2\%$ for 1.8 kA m^{-2}. The obtained energy efficiency at low current densities is within

a range of the current commercial water electrolyzers [51, 52]. In the case of 2.5 mol L^{-1}, no irreversible degradation of electrolytic cell parts was noticed. The reduced conductivity of the electrolytic cell in the case of the 4 mol L^{-1} catholyte requires significantly higher potential at comparable current densities. All these together lead to additional negative effects not only on the efficiency through HER, but also on performance and degradation of the electrolysis system parts. We observed an increased system heating, a minor DSA® anode deterioration, Fe deposition on the membrane, and, consequently, irreversible membrane degradation.

To establish the relationship between the current density and energy efficiency, the electrolysis experiments were performed with different current densities (j) ranging from 0.1 to 1.8 kA m^{-2} and at the system temperature of 70 °C. The relationship between the current density and applied potential is almost linear or even slightly exponential (see bottom figures in Fig. 3), revealing that the electrolysis under such conditions is not controlled by the concentration polarization. This is expected due to the high electrolyte concentrations and intense agitation of the electrolyte by recirculation through the electrolytic cell. This makes the mass transport of ionic species, from the bulk electrolyte to the electrode surface, fast enough to minimize the boundary diffusion layer, as well as to remove bubbles and limit their masking effect [53, 54].

The energy efficiency-current density curves in Fig. 4 can be fitted with an equation

$$\eta_e(j) = \frac{1}{(1 + a\ln(j) + bj)} \quad (4)$$

where a and b are fitting coefficients and the terms $a\ln(j)$ and bj represent energy losses due to the activation and resistance polarization, respectively. In Table 1, one can observe an increase in the contribution of resistance polarization with the current density and an increase in the contribution of activation polarization with the catholyte concentration. The fit, using Eq. (4), shows that for 1 mol L^{-1} catholyte the resistance polarization contributes to 18.2% share at the lowest current density and 67.8% at the highest, while the 2.5 mol L^{-1} accounts for 40.4% for the lowest and increases to 88.2% share of the energy efficiency losses for the highest current density. The contribution of activation polarization

Table 1 The obtained activation (a) and resistance (b) coefficients and the calculated activation (act. %) and resistance (res. %) loss shares at current densities of 0.1, 1.5, and 1.8 kA m^{-2} for 1, 2.5, and 4 mol L^{-1} catholyte concentration (C)

C [mol L^{-1}]	a	b	0.1 kA m^{-2}		1.5 kA m^{-2}		1.8 kA m^{-2}	
			act. %	res. %	act. %	res. %	act. %	res. %
1	0.0390	0.0004	81.8%	18.2%	32.2%	67.8%	-	-
2.5	0.0160	0.0005	59.6%	40.4%	13.5%	86.5%	11.8%	88.2%
4	0.0008	0.0030	1.2%	98.8%	0.1%	99.9%	-	-
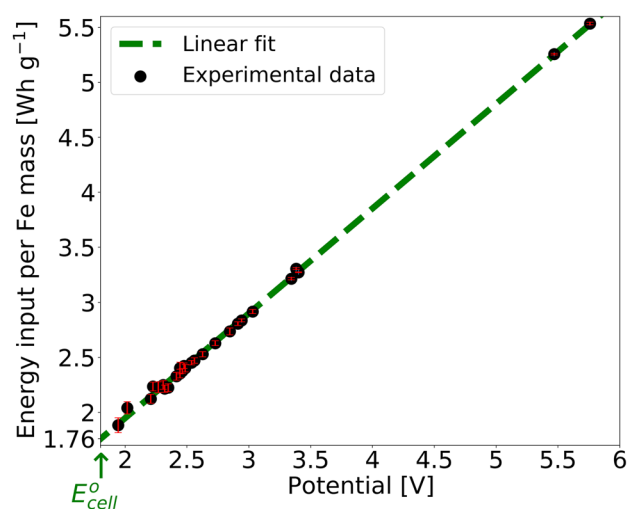
Fig. 6 The black dots represent experimental energy input per mass of Fe deposit as a function of the potential. A linear fit of the experimental data is marked with a green dashed line and is extrapolated toward E_{cell}

is found to be almost negligible for the 4 mol L^{-1} catholyte over the entire current density range. Consequently, the resistance polarization accounts for almost 100% of the losses for 4 mol L^{-1}.

The efficiency of the electrolysis can be expressed also as the energy input per mass of deposited iron (Wh g^{-1}). According to Eq. 1, it is obvious that the energy efficiency optimization must involve lowering the electrolytic cell resistance since it governs the relationship between potential and current density. In other words, the potential required for electrodeposition at a certain current density should be minimized to lower the energy losses due to the Joule heating effect. Our results (Fig. 6) show a very linear dependence between the energy input and potential. The lowest energy input per mass of Fe deposit that we have reached is 1.88 (± 0.09) Wh g^{-1} at a current density of 102 A m^{-2} and an average potential of 1.94 V, when running the electrolysis of 2.5 mol L^{-1} FeCl$_2$ (aq) at 70 °C. The limiting energy input, obtained by extrapolation towards $E_{\text{cell}}^{\text{o}}$, was found to be 1.76 Wh g^{-1}. At the elevated temperature, the energy input can even be slightly lower, which can only be reached using optimized electrodeposition conditions at potential infinitesimal higher than the cell potential.

Conclusions

Here we focused on the electrolysis energy efficiency of highly concentrated FeCl$_2$ aqueous solutions as a function of catholyte concentration, system temperature, and current density. We

showed that cell conductivity has a dominant influence on the energy efficiency of the electrolytic process. The conductivity of the FeCl$_2$ solution peaks at 2.25 mol L^{-1} and strongly increases with temperature. However, despite a significant difference in conductivity, the 1 and 2 mol L^{-1} catholyte gave very similar electrolysis energy efficiency. This indicates yet another important contribution, i.e., the conductivity of the ion-exchange membrane. The system temperature is directly proportional to the electrolytic cell conductivity, and it lowers the potential at a specific current density. As a consequence, the energy efficiency increases with temperature by about 0.3% per degree. The use of such catholyte solution at a system temperature of 70 °C resulted in the highest energy efficiency of 89 $\pm$ 3% at a current density of 0.1 kA m^{-2} and monotonically decreased to 51 $\pm$ 2% at 1.8 kA m^{-2}. The lowest energy input per mass unit of deposited Fe that we have obtained is 1.88 (± 0.09) Wh g^{-1} at the current density of 0.1 kA m^{-2}, the potential of 1.94 V, and system temperature of 70 °C. The extrapolation of the results towards $E_{\text{cell}}^{\text{o}}$ gives the minimum energy input per mass unit of Fe deposit to be 1.76 Wh g^{-1}.

The nearly linear dependence between the potential and current density proves that the mass transport of ionic species from the bulk electrolyte to the electrode surface is not a rate-limiting step in our system. Consequently, we fitted the experimental results with two free parameters, $a\ln(j)$ and bj, for activation and resistance polarization, respectively. For 2.5 mol L^{-1}, the resistance polarization accounts for 40.4% of the overall energy efficiency losses for the lowest current density and increases to 88.2% share for the highest current density. For 2.5 mol L^{-1}, the first traces of the hydrogen-evolving reaction were noticed at the current density of 1.8 kA m^{-2}. The activation polarization was found almost negligible for 4 mol L^{-1} over the entire current density range. For 4 mol L^{-1}, the current efficiency dropped to 80 $\pm$ 2% due to secondary HER at a current density of 1.5 kA m^{-2}. For 1 and 2.5 mol L^{-1} catholyte, no irreversible degradation of electrolytic cell parts was noticed. Furthermore, to minimize the efficiency losses and prevent system degradation at high current densities, the catholyte concentration must be well below 4 mol L^{-1} FeCl$_2$.

Declarations

References

1. Fares RL, Webber ME (2017) Reduce reliance on the utility. Nat Energy 2:1

2. Rawea AS, Urooj S (2018) Strategies, current status, problems of energy and perspectives of Yemen's renewable energy solutions. Renew Sustain Energy Rev 82:1655–1663. https://doi.org/10.1016/j.rser.2017.07.015

3. Revesz RL, Unel B (2018) Managing the future of the electricity grid: energy storage and greenhouse gas emissions. Harvard Environ Law Rev 42:139–196

4. Valant M (2021) Procedure for electric energy storage in solid matter. United States Patent and Trademark Office. Patent No. US20200308715

5. Ulrichson D~L, Yeh Y~S (1975) Thermochemical water splitting: the reverse Deacon reaction and alternatives. 11541

6. O'Brien TF, Bommaraju TV, Hine F (2005) Handbook of chlor-alkali technology, vol 1

7. Beckmann R, Lüke B (2000) Know-how and technology-improving the return on investment for conversions, expansions and new chlorine plants. In: Moorhouse J (ed) Modern chlor-alkali technology, pp 196–212

8. Brinkmann T, Giner Santonja G, Schorcht F et al (2014) Best available techniques reference document for the production of chlor-alkali

9. Lakshmanan S, Murugesan T (2013) The chlor-alkali process: work in progress. Clean Technol Environ Policy 16:225–234

10. Zhang Z, Kitada A, Fukami K et al (2020) Electrodeposition of an iron thin film with compact and smooth morphology using an ethereal electrolyte. Electrochim Acta 348:136289. https://doi.org/10.1016/j.electacta.2020.136289

11. Yitzhack N, Tereschuk P, Sezin N et al (2020) Aluminum electrodeposition from a non-aqueous electrolyte—a combined computational and experimental study. J Solid State Electrochem 24:2833–2846. https://doi.org/10.1007/s10008-020-04626-x

12. Hallett JP, Welton T (2011) Room-temperature ionic liquids: solvents for synthesis and catalysis. 2. Chem Rev 111:3508–3576. https://doi.org/10.1021/cr1003248

13. Smith EL, Abbott AP, Ryder KS (2014) Deep eutectic solvents (DESs) and their applications. Chem Rev 114:11060–11082. https://doi.org/10.1021/cr300162p

14. Brooman EW (2007) Ionic liquids for surface finishing processes. Plat Surf Finish 94:54–57

15. Panzeri G, Muller D, Accogli A et al (2019) Zinc electrodeposition from a chloride-free non-aqueous solution based on ethylene glycol and acetate salts. Electrochim Acta 296:465–472. https://doi.org/10.1016/j.electacta.2018.11.060

16. Lipsztajn M, Osteryoung RA (1985) Electrochemistry in neutral ambient-temperature ionic liquids. 1. Studies of iron(III), neodymium(III), and lithium(I). Inorg Chem 24:716–719. https://doi.org/10.1021/ic00199a016

17. Giridhar P, Weidenfeller B, El Abedin SZ, Endres F (2014) Electrodeposition of iron and iron-aluminium alloys in an ionic liquid and their magnetic properties. Phys Chem Chem Phys 16:9317–9326. https://doi.org/10.1039/c4cp00613e

18. Castrillejo Y, Martinez AM, Vega M, Batanero PS (1996) Electrochemical reduction of Fe (ii) ions on different solid electrodes in fused ZnCl 2–2NaCl mixture. J Appl Electrochem 26:1279–1285

19. Lugovskoy A, Zinigrad M, Aurbach D, Unger Z (2009) Electrodeposition of iron(II) on platinum in chloride melts at 700–750oC. Electrochim Acta 54:1904–1908

20. Pye S, Winnick J, Kohl PA (1997) Iron, copper, and nickel behavior in buffered, neutral aluminum chloride: 1-methyl-3-ethylimidazolium chloride molten salt. J Electrochem Soc 144:1933–1938. https://doi.org/10.1149/1.1837724

21. Thomas BK, Fray DJ (1982) The conductivity of aqueous zinc chloride solutions. J Appl Electrochem 12:1–5

22. Agmon N (1995) The Grotthuss mechanism. Chem Phys Lett 244:456–462. https://doi.org/10.1016/0009-2614(95)00905-J

23. de Grotthuss CJT (1806) Sur la décomposition de l'eau et des corps qu'elle tient en dissolution à l'aide de l'électricité galvanique. Ann Chim 58:54–73

24. Lamb AB, Elder LW (1931) The electromotive activation of oxygen. J Am Chem Soc 53:137–163. https://doi.org/10.1021/ja01352a019

25. Denbigh KG, Hicks M, Page FM (1948) The kinetics of open reaction systems. Trans Faraday Soc 44:479–494. https://doi.org/10.1039/TF9484400479

26. Oh ST, Joo MH, Choa YH et al (2010) Synthesis of Fe(Ni) nanoparticles by calcination and hydrogen reduction of metal nitrate powders. Phys Scr. https://doi.org/10.1088/0031-8949/2010/T139/014050

27. Strmcnik D, Uchimura M, Wang C et al (2013) Improving the hydrogen oxidation reaction rate by promotion of hydroxyl adsorption. Nat Chem 5:300–306. https://doi.org/10.1038/nchem.1574

28. Sheng W, Myint M, Chen JG, Yan Y (2013) Correlating the hydrogen evolution reaction activity in alkaline electrolytes with the hydrogen binding energy on monometallic surfaces. Energy Environ Sci 6:1509–1512. https://doi.org/10.1039/C3EE00045A

29. Ledezma-Yanez I, Wallace WDZ, Sebastián-Pascual P et al (2017) Interfacial water reorganization as a pH-dependent descriptor of the hydrogen evolution rate on platinum electrodes. Nat Energy 2:1–7. https://doi.org/10.1038/nenergy.2017.31

30. Duby P (1980) The history of progress in dimensionally stable anodes

31. Trasatti S (2000) Electrocatalysis: understanding the success of DSA®. Electrochim Acta 45:2377–2385. https://doi.org/10.1016/S0013-4686(00)00338-8

32. Karlsson RKB, Cornell A (2016) Selectivity between oxygen and chlorine evolution in the chlor-alkali and chlorate processes. Chem Rev 116:2982–3028. https://doi.org/10.1021/acs.chemrev.5b00389

33. Dong H, Yu W, Hoffmann MR (2021) Mixed metal oxide electrodes and the chlorine evolution reaction. J Phys Chem C 125:20745–20761. https://doi.org/10.1021/acs.jpcc.1c05671

34. Janssen LJJ, Starmans LMC, Visser JG, Barendrecht E (1977) Mechanism of the chlorine evolution on a ruthenium oxide/titanium oxide electrode and on a ruthenium electrode. Electrochim Acta 22:1093–1100. https://doi.org/10.1016/0013-4686(77)80045-5

35. Takasu Y, Sugimoto W, Nishiki Y, Nakamatsu S (2010) Structural analyses of RuO 2-TiO 2/Ti and IrO 2-RuO 2-TiO 2/Ti anodes used in industrial chlor-alkali membrane processes. J Appl Electrochem 40:1789–1795. https://doi.org/10.1007/s10800-010-0137-3

36. Li K, Fan Q, Chuai H et al (2021) Revisiting chlor-alkali electrolyzers: from materials to devices. Trans Tianjin Univ 27:202–216. https://doi.org/10.1007/s12209-021-00285-9

37. Vos JG, Liu Z, Speck FD et al (2019) Selectivity trends between oxygen evolution and chlorine evolution on iridium-based double

perovskites in acidic media. ACS Catal 9:8561–8574. https://doi.org/10.1021/acscatal.9b01159

38. Izaki M (2010) Electrodeposition of iron and iron alloys. In: Modern electroplating. John Wiley & Sons, Ltd, pp 309–326

39. Noon CW (1947) Electro-deposition of iron from a chloride bath. 227

40. Jeon SH, Song GD, Hur DH (2016) Effects of deposition potentials on the morphology and structure of iron-based films on carbon steel substrate in an alkaline solution. Adv Mater Sci Eng. https://doi.org/10.1155/2016/9038478

41. Maksimović VM, Pavlović LJ, Jović BM, Pavlović MG (2008) Electrodeposition of Fe powder from acid electrolytes. J Serbian Chem Soc 73:861–870. https://doi.org/10.2298/JSC0809861M

42. Thomas JD, Klingenmaier OJ, Hardesty DW (1969) Iron plating—process and product characteristics. Trans IMF 47:209–216. https://doi.org/10.1080/00202967.1969.11870115

43. Pavlović LJ, Pavlović MM, Pavlović MG et al (2010) Electrodeposition of Fe powder from citrate containing electrolytes. Int J Electrochem Sci 5:1898–1910

44. Levy SI (1930) Electrolysis of ferrous chloride. United States Patent Office No.: 1752348

45. Cardarelli F, Lefebvre S, Tousignant C, Hudon G (2008) Electrochemical process for the recovery of metallic iron and chloride values from iron-rich metal chloride wastes. U.S.P.A. PCT/CA2007/000026

46. Isono T (1984) Density, viscosity, and electrolytic conductivity of concentrated aqueous electrolyte solutions at several temperatures. Alkaline-earth chlorides, LaCl3, Na2SO4, NaNO3, NaBr, KNO3, KBr, and Cd(NO3)2. J Chem Eng Data 29:45–52

47. Luin U, Arčon I, Valant M (2022) Structure and population of complex ionic species in FeCl2 aqueous solution by X-ray absorption spectroscopy. Molecules. https://doi.org/10.3390/molecules27030642

48. Zhu S, Kingsbury RS, Call DF, Coronell O (2018) Impact of solution composition on the resistance of ion exchange membranes. J Memb Sci 554:39–47. https://doi.org/10.1016/j.memsci.2018.02.050

49. Díaz JC, Kamcev J (2021) Ionic conductivity of ion-exchange membranes: measurement techniques and salt concentration dependence. J Memb Sci 618:118718. https://doi.org/10.1016/j.memsci.2020.118718

50. Kamcev J, Sujanani R, Jang E-S et al (2018) Salt concentration dependence of ionic conductivity in ion exchange membranes. J Memb Sci 547:123–133. https://doi.org/10.1016/j.memsci.2017.10.024

51. Thyssenkrupp (2019) Hydrogen from large-scale electrolysis. 5. https://ucpcdn.thyssenkrupp.com/_legacy/UCPthyssenkruppBAISUhdeChlorineEngineers/assets.files/products/water_electrolysis/tk_19_0820_hydrogen_broschuere_2019_03.pdf. Accessed 14 Feb 2022

52. Bareiß K, de la Rua C, Möckl M, Hamacher T (2019) Life cycle assessment of hydrogen from proton exchange membrane water electrolysis in future energy systems. Appl Energy 237:862–872. https://doi.org/10.1016/j.apenergy.2019.01.001

53. Angulo A, van der Linde P, Gardeniers H et al (2020) Influence of bubbles on the energy conversion efficiency of electrochemical reactors. Joule 4:555–579. https://doi.org/10.1016/j.joule.2020.01.005

54. Swiegers GF, Terrett RNL, Tsekouras G et al (2021) The prospects of developing a highly energy-efficient water electrolyser by eliminating or mitigating bubble effects. Sustain Energy Fuels 5:1280–1310. https://doi.org/10.1039/D0SE01886D